Atmos. Chem. Phys. Discuss., https://doi.org/10.5194/acp-2019-76
Manuscript under review for journal Atmos. Chem. Phys.
Discussion started: 5 February 2019

Atmospheric Chemistry and Physics Discussions

Timescales of Secondary Organic Aerosols to Reach Equilibrium at Various Temperatures and Relative Humidities

Ying Li[1], and Manabu Shiraiwa[1,*]

[1] Department of Chemistry, University of California, Irvine, California, USA.

[*]Correspondence to: Manabu Shiraiwa (m.shiraiwa@uci.edu)

Atmos. Chem. Phys. Discuss., https://doi.org/10.5194/acp-2019-76
Manuscript under review for journal Atmos. Chem. Phys.
Discussion started: 5 February 2019

Atmospheric Chemistry and Physics Discussions

10 **Abstract:**

11 Secondary organic aerosols (SOA) account for a substantial fraction of air particulate
12 matter and SOA formation is often modeled assuming rapid establishment of
13 gas-particle equilibrium. Here, we estimate the characteristic timescale for SOA to
14 achieve gas−particle equilibrium under a wide range of temperatures and relative
15 humidities using a state-of-the-art kinetic flux model. Equilibration timescales were
16 calculated by varying particle phase state, size, mass loadings, and volatility of
17 organic compounds. Model simulations suggest that the equilibration timescale for
18 semi-volatile compounds is on the order of seconds or minutes for most conditions in
19 the planetary boundary layer, but it can be longer than one hour if particles adopt
20 glassy or amorphous solid states with high glass transition temperature at low relative
21 humidity. In the free troposphere with lower temperatures it can be longer than hours
22 or days even at moderate or relatively high RH due to kinetic limitations of bulk
23 diffusion in highly viscous particles. The timescale of partitioning of low-volatile
24 compounds is shorter compared to semi-volatile compounds, as it is largely
25 determined by condensation sink due to very slow re-evaporation. These results
26 provide critical insights into thermodynamic or kinetic treatments of SOA partitioning
27 for accurate predictions of gas- and particle-phase concentrations of semi-volatile
28 compounds in regional and global chemical transport models.

Atmos. Chem. Phys. Discuss., https://doi.org/10.5194/acp-2019-76
Manuscript under review for journal Atmos. Chem. Phys.
Discussion started: 5 February 2019

1. Introduction

Secondary organic aerosols (SOA) play a central role in climate, air quality and public health. Accurate descriptions of formation and evolution of SOA remain a grand challenge in climate and air quality models (Kanakidou et al., 2005; Shrivastava et al., 2017a). Current chemical transport models usually employ instantaneous equilibrium partitioning of semi-volatile oxidation products into the particle phase (Pankow, 1994), assuming that SOA partitioning is rapid compared to the timescales of other major atmospheric processes associated with SOA formation. The timescale of SOA to reach equilibrium with their surrounding condensable vapors needs to be evaluated under different ambient conditions to validate this assumption.

SOA particles can adopt liquid (dynamic viscosity $\eta < 10^2$ Pa s), semi-solid ($10^2 \leq \eta \leq 10^{12}$ Pa s), or glassy or amorphous solid states ($\eta > 10^{12}$ Pa s), depending on chemical composition, temperature (T) and relative humidity (RH) (Virtanen et al., 2010; Koop et al., 2011; Reid et al., 2018). The occurrence of glassy or amorphous solid states may lead to kinetic limitations and prolonged equilibration timescale in SOA partitioning (Shiraiwa and Seinfeld, 2012; Booth et al., 2014; Zaveri et al., 2014; Mai et al., 2015), affecting evolution of particle size distribution upon SOA growth (Maria et al., 2004; Shiraiwa et al., 2013a; Zaveri et al., 2018). A number of experimental studies have indeed observed kinetic limitations of the bulk diffusion of organic molecules (Vaden et al., 2011; Perraud et al., 2012; Zhang et al., 2018), while chamber experiments probing the intraparticle mixing did not find kinetic limitations

at moderate and high RH and room temperature (Ye et al., 2016; Gorkowski et al., 2017; Ye et al., 2018).

Recently, global simulations predicted that SOA particles are expected to be mostly in a glassy solid phase state in the middle and upper troposphere and also in dry lands in the boundary layer (Shiraiwa et al., 2017), which can lead to prolonged characteristic bulk diffusion timescales of organic molecules within SOA particles (Shiraiwa et al., 2011; Maclean et al., 2017). Slow bulk diffusion associated with a glassy phase state can prevent atmospheric oxidants to react with organic compounds such as polycyclic aromatic hydrocarbons (Shrivastava et al., 2017b; Mu et al., 2018), contributing to long-range transport of organic compounds. Recent ambient observations have shown that the condensation of highly oxygenated molecules (HOMs), which play an important role in new particle formation, would be governed by kinetic partitioning in the free troposphere (Bianchi et al., 2016). Diffusivity measurements of volatile organics in levitated viscous particles have shown strong temperature dependence of bulk diffusivity and evaporation timescale (Bastelberger et al., 2017). Slow bulk diffusion may impact multiphase processes such as browning of organic particles (Liu et al., 2018), cloud droplet activation (Slade et al., 2017), and ice nucleation pathways (Knopf et al., 2018).

Given these observations and strong implications of SOA phase states, it is important to evaluate common assumption of gas-particle partitioning equilibrium at different ambient conditions. In this study we provide theoretical analysis of partitioning kinetics of organic compounds using the kinetic multi-layer model of

Atmos. Chem. Phys. Discuss., https://doi.org/10.5194/acp-2019-76
Manuscript under review for journal Atmos. Chem. Phys.
Discussion started: 5 February 2019

gas-particle interactions in aerosols and clouds (KM-GAP) (Shiraiwa et al., 2012), which accounts for mass transport in both gas and particle phases. The equilibration timescale (τ_{eq}) of organic compounds partitioning into mono-dispersed particles is evaluated systematically under a wide range of temperatures and RH, considering the effects of particle phase state, particle size, mass loadings, and volatility of organic compounds.

2. Methods

We evaluate the timescale to achieve gas-particle equilibrium by simulating condensation of a compound Z into pre-existing non-volatile mono-dispersed particles using the KM-GAP model. KM-GAP consists of multiple model compartments and layers, respectively: gas phase, near-surface gas phase, sorption layer, surface layer, and a number of bulk layers (Shiraiwa et al., 2012). The following processes are treated as temperature-dependent in KM-GAP: gas phase diffusion, adsorption/desorption, surface-bulk exchange, and bulk diffusion (Fig. S1). The physical and kinetic parameters are summarized in Table S1. The gas-phase diffusion coefficient depends on both *T* and ambient pressure, which is chosen to match *T* in the International Standard Atmosphere. The adsorption rate coefficient is related to the mean thermal velocity as a function of *T* and the surface accommodation coefficient, which is assumed to be 1 (Julin et al., 2014). The *T*-dependence of desorption rate coefficient is described by an Arrhenius equation with an assumed typical adsorption enthalpy of 40 kJ mol^{-1}.

Atmos. Chem. Phys. Discuss., https://doi.org/10.5194/acp-2019-76
Manuscript under review for journal Atmos. Chem. Phys.
Discussion started: 5 February 2019

Phase state and viscosity can be characterized by the glass transition temperature (T_g), at which phase transition between amorphous solid and semi-solid states occurs (Koop et al., 2011). When T_g of organic particles under dry conditions ($T_{g,org}$) is known, T_g of organic-water mixtures at given RH can be estimated considering hygroscopic growth combined with the Gordon-Taylor equation. In this work, we assumed the effective hygroscopicity parameter κ as 0.1 (Petters and Kreidenweis, 2007; Gunthe et al., 2009) and the Gordon-Taylor constant as 2.5 (Koop et al., 2011). Then, the T-dependence of viscosity is calculated using the Vogel-Tammann-Fulcher equation (Angell, 1991; Rothfuss and Petters, 2017; DeRieux et al., 2018; Li and Shiraiwa, 2018).

Figure 1 shows the T- and RH-dependent viscosity of SOA particles with $T_{g,org}$ of (a) 240 K, (b) 270 K, and (c) 300 K. We chose these three $T_{g,org}$ values to represent different phase states of liquid, semi-solid, and glassy states, respectively, at T of 298 K under dry conditions and these values are within the range recently reported for monoterpene-derived SOA (Petters et al., 2019). The decrease of T leads to increase of viscosity, while the increase of RH leads to decrease of viscosity due to the plasticizing effect of water (Koop et al., 2011). The bulk diffusion coefficient D_b (Fig. S2) is calculated by the Stokes–Einstein equation, which has been shown to work very well for organic molecules diffusing through materials with viscosity below ~10^3 Pa s (Chenyakin et al., 2017). Note that the Stokes–Einstein equation may underpredict D_b in highly viscous SOA thus it gives lower limits of D_b (Marshall et al., 2016; Bastelberger et al., 2017; Reid et al., 2018). D_b is fixed at any given depth in the

Atmos. Chem. Phys. Discuss., https://doi.org/10.5194/acp-2019-76
Manuscript under review for journal Atmos. Chem. Phys.
Discussion started: 5 February 2019

particle bulk in each simulation, assuming that condensation of Z would not alter particle viscosity and diffusivity as only trace amounts of Z condense to pre-existing particles in our simulations.

We consider a closed system, in which condensation of Z would lead to a decrease of its gas-phase mass concentration (C_g) and an increase of its particle-phase mass concentration (C_p). The particle diameter stays practically constant throughout each simulation, as the amount of condesing Z is set to be much smaller than the non-volatile pre-existing particle mass (C_{OA}). The gas-phase mass concentration of Z right above the surface (C_s) is also calculated based on the Raoult's law and partitioning theory (Pankow, 1994) in equilibrium with the near-surface bulk, which is resolved by KM-GAP (Shiraiwa and Seinfeld, 2012). We also calculate the mass fraction of Z in the near-surface bulk (f_s) and the average mass fraction of Z in the entire bulk (f_b) to infer the radial concentration profile (Fig. S3). The equilibration timescale (τ_{eq}) is calculated as the e-folding time t when the following criterion is met,

$$\frac{|C_p(t) - C_{p,eq}|}{|C_{p,0} - C_{p,eq}|} < \frac{1}{e} \quad (1)$$

where $C_{p,0}$ and $C_{p,eq}$ are the initial and equilibrium mass concentration of Z in the particle phase, respectively. Note that practically the same values can also be obtained by using initial and equilibrium gas-phase concentrations in Eq. (1), as the mass change of Z in the gas and particle phases are the same in these simulations.

3 Results

Atmos. Chem. Phys. Discuss., https://doi.org/10.5194/acp-2019-76
Manuscript under review for journal Atmos. Chem. Phys.
Discussion started: 5 February 2019

Atmospheric Chemistry and Physics Discussions

Figure 2 shows exemplary simulations of temporal evolution of C_g (blue line) and C_p (red line) of the compound Z along with τ_{eq} marked with red circles. The initial mass concentration of pre-existing non-volatile mono-dispersed particles (C_{OA}) is assumed to be 20 μg m^{-3} with the number concentrations of 3 × 10^4 cm^{-3} and the initial particle diameter of 100 nm. Initial mass concentrations of Z in the gas ($C_{g,0}$) and particle ($C_{p,0}$) phases are set to be 0.3 μg m^{-3} and 0 μg m^{-3}, respectively. $T_{g,org}$ is assumed to be 270 K. Figure 2a presents simulations for a semi-volatile compound (SVOC, C_0 = 10 μg m^{-3}) at RH = 60% and T = 298 K with D_b of 10^{-11} cm^2 s^{-1} (Fig. S2). Upon condensation C_g decreases, while C_s and C_p increase, and the gas-particle equilibrium is reached within about 20 s as indicated by τ_{eq}. For low-volatile organic compounds (LVOC) with C_0 = 0.1 μg m^{-3}, it takes longer time to reach the equilibrium with τ_{eq} of ~30 s (Fig. 2b), as the partial pressure gradient between the gas phase and the particle surface (represented by the difference between C_g and C_s) is larger for lower C_0. For both cases SOA growth is governed by gas-phase diffusion as indicated by $C_s < C_g$. The mass fraction of Z in the near-surface bulk is identical to the average mass fraction in the entire bulk (Fig. S3 a–b), indicating that Z are homogeneously well-mixed in the particle without kinetic limitations of bulk diffusion in low viscous particles (Fig. 3a).

At lower T of 250 K, the phase state of pre-existing particles occurs as highly viscous with D_b of ~10^{-18} cm^2 s^{-1} (Fig. S2), resulting in much longer equilibration timescales (~10^5 s) for SVOC with C_0 = 10 μg m^{-3} (Fig. 2c). After C_g and C_s converge, they continue to decrease simultaneously while C_p increases slowly,

159 showing that the particle undergoes quasi-equilibrium growth (Shiraiwa and Seinfeld,
160 2012; Zhang et al., 2012). For LVOC (C_0 = 0.1 μg m^{-3}) condensation, τ_{eq} is short
161 (~140 s) because of a local thermodynamic equilibrium between the gas phase and the
162 near-surface bulk established relatively quickly (as mostly controlled by the
163 condensation sink: Riipinen et al., 2011; Tröstl et al., 2016) due to very slow
164 re-evaporation of LVOC.

165 The characteristic timescale of mass transport and mixing by molecular
166 diffusion τ_{mix} can be calculated by $\tau_{mix} = r_p^2 / (\pi^2 D_b)$, where r_p is the particle radius
167 (Seinfeld and Pandis, 2006). Figure 3 shows dimensionless radial concentration
168 profiles of Z (C_0 = 0.1 μg m^{-3}) in the particle at (a) $D_b = 10^{-11}$ cm^2 s^{-1} and (b) 10^{-18} cm^2
169 s^{-1}, respectively. For low viscous particles, τ_{mix} is very short and particles are
170 homogeneously well-mixed at τ_{eq}. In contrast, there exists a large concentration
171 gradient between the particle surface and the inner bulk (Fig. 3b, S3d) at τ_{eq} in highly
172 viscous particles due to strong kinetic limitations of bulk diffusion (as indicated by
173 very long τ_{mix}), which prevents the entire particle bulk to reach complete equilibrium.
174 Thus, for LVOC condensation on highly viscous particles (Fig. 2d), τ_{mix} represents the
175 timescale to establish full equilibrium with homogeneous mixing in the entire particle
176 bulk. These results are consistent with Mai et al. (2015) and Liu et al. (2016), which
177 showed that an establishment of full equilibrium is limited by bulk diffusion in highly
178 viscous particles, even though the local equilibrium of LVOC may be achieved faster.
179 Note that τ_{mix} is solely a function of particle size and bulk diffusivity, while τ_{eq} is also
180 affected by volatility and mass loadings. At lower particle concentrations, the total

Atmos. Chem. Phys. Discuss., https://doi.org/10.5194/acp-2019-76
Manuscript under review for journal Atmos. Chem. Phys.
Discussion started: 5 February 2019

accommodation of molecules to the particle surface decreases, resulting in longer equilibration timescales (Fig. S4).

We also simulated evaporation in the closed system with same parameters as the condensation simulations (Table S2). Initially C_g = 0 and trace amounts of semi-volatile or low-volatile species were assumed to be homogeneously well-mixed in pre-existing particles. Figure S5 shows that for the evaporation of SVOC species with C_0 = 10 μg m^{-3}, decreasing D_b from 10^{-11} cm^2 s^{-1} to 10^{-18} cm^2 s^{-1} would increase τ_{eq} from ~ 20 s to ~ 10^5 s. These evaporation timescales are close to those derived from condensation (Fig. 2a,c) and consistent with previous kinetic simulations (Liu et al., 2016). In the closed system, the evaporation of a very small amount of LVOC species from the particle surface is already sufficient to reach the particle-phase equilibrium concentration, resulting in a short τ_{eq} (Fig. S5b,d). For an open system with continuous removal of gas-phase compounds, which has been employed in evaporation experiments, the equilibrium timescale in the evaporation of the LVOC species from highly viscous particles can be longer than hours or days (Vaden et al., 2011; Liu et al., 2016).

We conducted further simulations to estimate equilibration timescales (τ_{eq}) with a wide range of atmospherically-relevant temperatures (220 - 310 K) and relative humidities (0 - 100%). Figure 4 shows the temperature and humidity-dependent diagrams of τ_{eq} for SVOC (C_0 = 10 μg m^{-3}) condensation on particles with $T_{g,org}$ of 240 K, 270 K, and 300 K, respectively. For particles with $T_{g,org}$ of 240 K (panel a), τ_{eq} is on the order of seconds under boundary layer conditions (T > 270 K). In these

Atmos. Chem. Phys. Discuss., https://doi.org/10.5194/acp-2019-76
Manuscript under review for journal Atmos. Chem. Phys.
Discussion started: 5 February 2019

conditions particles are liquid with high bulk diffusivity (Fig. 1a and S2a), thus gas-particle partitioning is controlled by gas-phase diffusion and interfacial transport (Shiraiwa and Seinfeld, 2012; Mai et al., 2015). At low T (< 260 K) with low or moderate RH (< 70%), τ_{eq} can increase from minutes to one year with decreasing T and RH mainly due to strong kinetic limitations of bulk diffusion with low D_b (Fig. S2a). With $T_{g,org}$ of 270 K (panel b) or 300 K (panel c), τ_{eq} is still on the order of minutes in most of boundary layer conditions. At low RH τ_{eq} can be extended to hours when particles may occur as amorphous (semi-)solid. When T < 270 K, τ_{eq} can be longer than months even at moderate RH, while τ_{eq} may stay very short at very high RH.

τ_{eq} for $C_0 = 10^3$ and 0.1 μg m^{-3} are presented in Fig. A1. In general, τ_{eq} would be shorter at higher C_0, as the partial pressure gradient between the gas phase and the particle surface is smaller for higher C_0 (Shiraiwa and Seinfeld, 2012; Liu et al., 2016). For example, the increase of C_0 from 10 μg m^{-3} to 10^3 μg m^{-3} leads to τ_{eq} decrease from 30 s to 1 s with $T_{g,org}$ of 240 K at boundary layer conditions (Fig. 4a, A1a). At low T and RH (e.g., T < 250 K and RH < 50 %) where particles are highly viscous, τ_{eq} is on the same order of magnitude for the condensation of IVOC and SVOC, as gas-particle partitioning is limited by bulk diffusion. Figure A2 shows bulk diffusion and mixing timescales (τ_{mix}) as a function of RH and T. It is interesting to note that τ_{mix} is very similar to τ_{eq} of IVOC (Fig. A1(a-c)) as gas diffusion and interfacial transport of IVOC are fast. For LVOC τ_{eq} is shorter than τ_{mix} as its mass transfer to the particle surface is governed by condensation sink with negligible

re-evaporation, while τ_{mix} is still long to achieve homogeneous mixing in the particle phase if particles are viscous.

Figure 5 shows the dependence of τ_{eq} of LVOC (C_0 = 0.1 μg m^{-3}) on the mass concentration and the diameter of pre-existing particles, over the range of 0.1 – 100 μg m^{-3} and 30 – 1000 nm, respectively, with particle phase state to be less viscous with $D_b = 10^{-11}$ cm^2 s^{-1} at 298 K and highly viscous with $D_b = 10^{-18}$ cm^2 s^{-1} at 250 K. In this comparison, when ambient particle mass concentration is held constant, increasing particle size will translate to a decrease of the number and surface area concentration of particles, and a decrease of total accommodation of molecules to the particle surface, thereby leading to an increase of τ_{eq}. When particle diameter is held constant, an increase of particle concentration leads to an increase of surface area concentration, resulting in shorter τ_{eq}. Transition of the particle phase state from less viscous at 298 K ($D_b = 10^{-11}$ cm^2 s^{-1}) to highly viscous at 250 K ($D_b = 10^{-18}$ cm^2 s^{-1}) leads to longer τ_{eq}. Particles in nucleation mode (diameter < 30 nm) are not considered in this study, as the particle size may affect the phase transition of these nanoparticles (Cheng et al., 2015). The role and impact of phase transition on nucleation and growth of ultrafine particles are beyond the scope of current simulations and need further investigations in future studies.

4 Discussion

The timescale to reach equilibrium for SOA partitioning has been investigated in several laboratory experiments at room temperatures (Vaden et al., 2011; Saleh et al., 2013; Liu et al., 2016; Gong et al., 2018; Ye et al., 2018). These experiments monitored particle mass or composition, finding that equilibration timescales are longer at low RH, consistent with our model simulations. Note that, for condensation on highly viscous particles, even though particle mass or particle-phase concentrations appear to reach equilibrium, complete equilibrium with homogeneous mixing in the particle may not have been reached driven by strong kinetic limitations and concentration gradients in the particle bulk (Fig. 2d and 3b). This is also supported by evaporation experiments showing that the local thermodynamic equilibrium established between the vapor and the near-surface bulk should be differentiated from the global equilibrium between the vapor and the entire bulk (Liu et al., 2016). Note that SOA evaporation is also influenced by volatility and oligomer decomposition (Roldin et al., 2014; Yli-Juuti et al., 2017). Thus, particular care needs to be taken in comparing modeling results with different experiments on probing equilibration timescale (i.e., evaporation vs. condensation, open vs. closed system, local vs. full equilibrium).

The simulated equilibration timescales of atmospheric SOA are mostly on the order of minutes to hours under conditions of atmospheric boundary layer (Fig. 4, A1). This agrees with previous experimental results that the gas-particle interactions can be regulated by both thermodynamic and kinetic partitioning (Booth et al., 2014; Liu et al., 2016; Saha and Grieshop, 2016; Gong et al., 2018), depending on several

267 factors including particle phase state, size, mass loadings, and volatility. Organic
268 particles containing high molar-mass compounds tend to have high glass transition
269 temperatures (Koop et al., 2011) and the occurrence of kinetic limitation will increase
270 with higher $T_{g,org}$ (Fig. 4). This is consistent with the results of intraparticle mixing
271 experiments showing that as the carbon number of precursor (e.g. terpene) increased
272 (that would lead to higher $T_{g,org}$), it took longer time for SVOCs (evaporated from
273 another type of SOA, e.g. toluene SOA) to partition into the terpene SOA, leading to
274 slower molecular exchange among different types of SOA (Ye et al., 2018).

275 At low temperatures, the particles can occur as highly viscous at relatively
276 high RH (Fig. 1), and τ_{eq} can be longer than hours or days (Fig. 4, A1). Equilibration
277 timescales of LVOC condensation at low particle mass loadings (Fig. 5) may
278 represent the clean conditions where new particle formation and growth often occur
279 (Wang et al., 2016). It has been reported that highly oxygenated molecules play an
280 important role in the initial growth of atmospheric particles in the free troposphere
281 (Bianchi et al., 2016). Bulk diffusion would likely to be a limiting step in the
282 condensation of semi-volatile and low volatility compounds at low temperatures,
283 where particles may occur as highly viscous (Shiraiwa et al., 2017). In this case,
284 particle growth would need to be treated kinetically, rather than thermodynamic
285 equilibrium partitioning, as it would affect SOA growth kinetics and size distribution
286 dynamics, with significant implications for the growth of ultrafine particles to
287 climatically relevant sizes (Riipinen et al., 2011; Riipinen et al., 2012; Shiraiwa et al.,
288 2013a; Zaveri et al., 2018). Note that condensation of extremely low volatility organic

compounds (ELVOC; Tröstl et al., 2016) may be governed by gas-phase diffusion and timescales to reach local equilibrium could be shorter as determined by the condensation sink (Riipinen et al., 2011) (see also Fig. S4b), which may be more relevant for the practical application in chemical transport models.

In this study we assume that the bulk diffusivity within organic particles is independent of particle mixing state and morphology. Chamber experiments have demonstrated that evaporation of organic aerosol may be hindered if it is coated with organic aerosol from a different precursor (Loza et al., 2013; Boyd et al., 2017). Moreover, the phase separation has been observed in organic particles mixed with inorganic salts (You et al., 2014) and even without inorganic salts (Pöhlker et al., 2012; Riedel et al., 2016). Future simulations on equilibration timescale should consider the effects of the immiscibility (Barsanti et al., 2017) and the phase separation (Pye et al., 2017; Fowler et al., 2018) as well as composition-dependent bulk diffusivity (O'Meara et al., 2016) and the evolution of the particle phase due to reactive uptake and condensed-phase chemistry (Hosny et al., 2016). Particle size dependent phase transition (Cheng et al., 2015) and phase change in the course of particle growth (Shiraiwa et al., 2013b) may also need to be considered. The shift in particle phase state and gas-particle partitioning in response to temperature and RH may need to be considered in chemical transport models and laboratory experiments to better understand the fate of organic compounds.

Author contribution.

YL and MS designed and conducted modeling and wrote the manuscript.

Acknowledgments.

This work was funded by the National Science Foundation (AGS-1654104) and the Department of Energy (DE-SC0018349). The simulation data may be obtained from the corresponding author upon request.

References

Angell, C.: Relaxation in liquids, polymers and plastic crystals—strong/fragile patterns and problems, ,31 Cryst. Solids, 131, 13 J. Non https://doi.org/10.1016/0022-3093(91)90266-9, 1991.

Barsanti, K. C., Kroll, J. H. and Thornton, J. A.: Formation of low-volatility organic compounds in the atmosphere: recent advancements and insights, J. Phys. Chem. Lett., 8, 1503-1511, https://doi.org/10.1021/acs.jpclett.6b02969, 2017.

Bastelberger, S., Krieger, U. K., Luo, B. and Peter, T.: Diffusivity measurements of volatile organics in levitated viscous aerosol particles, Atmos. Chem. Phys., 17, 8453-8471, https://doi.org/10.5194/acp-17-8453-2017, 2017.

Bianchi, F., Tröstl, J., Junninen, H., Frege, C., Henne, S., Hoyle, C. R., Molteni, U., Herrmann, E., Adamov, A. and Bukowiecki, N.: New particle formation in the free troposphere: A question of chemistry and timing, Science, 352, 1109-1112, https://doi.org/10.1126/science.aad5456, 2016.

Booth, A. M., Murphy, B., Riipinen, I., Percival, C. J. and Topping, D. O.: Connecting bulk viscosity measurements to kinetic limitations on attaining equilibrium for a model aerosol composition, Environ. Sci. Technol., 48, 9298-9305, 10.1021/es501705c, 2014.

Boyd, C. M., Nah, T., Xu, L., Berkemeier, T. and Ng, N. L.: Secondary organic aerosol (SOA) from nitrate radical oxidation of monoterpenes: effects of temperature, dilution, and humidity on aerosol formation, mixing, and evaporation, Environ. Sci. Technol., 51, 7831-7841, https://doi.org/10.1021/acs.est.7b01460, 2017.

Cheng, Y., Su, H., Koop, T., Mikhailov, E. and Pöschl, U.: Size dependence of phase transitions in aerosol nanoparticles, Nat. Commun., 6, 5923, https://doi.org/10.1038/ncomms6923, 2015.

Chenyakin, Y., Ullmann, D. A., Evoy, E., Renbaum-Wolff, L., Kamal, S. and Bertram, A. K.: Diffusion coefficients of organic molecules in sucrose–water

345 solutions and comparison with Stokes–Einstein predictions, Atmos. Chem.
346 Phys., 17, 2423-2435, https://doi.org/10.5194/acp-17-2423-2017, 2017.

347 DeRieux, W. S. W., Li, Y., Lin, P., Laskin, J., Laskin, A., Bertram, A. K.,
348 Nizkorodov, S. A. and Shiraiwa, M.: Predicting the glass transition
349 temperature and viscosity of secondary organic material using molecular
350 composition, Atmos. Chem. Phys., 18, 6331-6351,
351 https://doi.org/10.5194/acp-18-6331-2018, 2018.

352 Fowler, K., Connolly, P. J., Topping, D. O. and O'Meara, S.: Maxwell–Stefan
353 diffusion: a framework for predicting condensed phase diffusion and phase
354 separation in atmospheric aerosol, Atmos. Chem. Phys., 18, 1629-1642,
355 https://doi.org/10.5194/acp-18-1629-2018, 2018.

356 Gong, Z., Han, Y., Liu, P., Ye, J., Keutsch, F. N., McKinney, K. A. and Martin, S. T.:
357 Influence of particle physical state on the uptake of medium-sized organic
358 molecules, Environ. Sci. Technol., 52, 8381-8389,
359 https://doi.org/10.1021/acs.est.8b02119, 2018.

360 Gorkowski, K., Donahue, N. M. and Sullivan, R. C.: Emulsified and liquid–liquid
361 phase-separated states of α-pinene secondary organic aerosol determined using
362 aerosol optical tweezers, Environ. Sci. Technol., 51, 12154-12163,
363 https://doi.org/10.1021/acs.est.7b03250, 2017.

364 Gunthe, S. S., King, S. M., Rose, D., Chen, Q., Roldin, P., Farmer, D. K., Jimenez, J.
365 L., Artaxo, P., Andreae, M. O., Martin, S. T. and Pöschl, U.: Cloud
366 condensation nuclei in pristine tropical rainforest air of Amazonia:
367 size-resolved measurements and modeling of atmospheric aerosol composition
368 and CCN activity, Atmos. Chem. Phys., 9, 7551-7575,
369 https://doi.org/10.5194/acp-9-7551-2009, 2009.

370 Hosny, N., Fitzgerald, C., Vyšniauskas, A., Athanasiadis, A., Berkemeier, T., Uygur,
371 N., Pöschl, U., Shiraiwa, M., Kalberer, M. and Pope, F.: Direct imaging of
372 changes in aerosol particle viscosity upon hydration and chemical aging,
373 Chem. Sci., 7, 1357-1367, https://doi.org/10.1039/C5SC02959G, 2016.

374 Julin, J., Winkler, P. M., Donahue, N. M., Wagner, P. E. and Riipinen, I.: Near-unity
375 mass accommodation coefficient of organic molecules of varying structure,
376 Environ. Sci. Technol., 48, 12083-12089, https://doi.org/10.1021/es501816h,
377 2014.

378 Kanakidou, M., Seinfeld, J., Pandis, S., Barnes, I., Dentener, F., Facchini, M.,
379 Dingenen, R. V., Ervens, B., Nenes, A. and Nielsen, C.: Organic aerosol and
380 global climate modelling: a review, Atmos. Chem. Phys., 5, 1053-1123,
381 https://doi.org/10.5194/acp-5-1053-2005, 2005.

382 Knopf, D. A., Alpert, P. A. and Wang, B.: The role of organic aerosol in atmospheric
383 ice nucleation: a review, ACS Earth Space Chem., 2, 168-202,
384 https://doi.org/10.1021/acsearthspacechem.7b00120, 2018.

385 Koop, T., Bookhold, J., Shiraiwa, M. and Poschl, U.: Glass transition and phase state
386 of organic compounds: dependency on molecular properties and implications
387 for secondary organic aerosols in the atmosphere, Phys. Chem. Chem. Phys.,
388 13, 19238-19255, https://doi.org/10.1039/C1CP22617G, 2011.

389 Li, Y. and Shiraiwa, M.: Molecular corridors, volatility and particle phase state in
390 secondary organic aerosols, in: Multiphase Environmental Chemistry in the
391 Atmosphere, edited by: Hunt S. W., Laskin A., and Nizkorodov S. A., ACS
392 Symposium Series, 1299, 209-244,
393 https://doi.org/10.1021/bk-2018-1299.ch011, 2018.

394 Liu, P., Li, Y. J., Wang, Y., Gilles, M. K., Zaveri, R. A., Bertram, A. K. and Martin,
395 S. T.: Lability of secondary organic particulate matter, Proc. Natl. Acad. Sci.
396 U.S.A., 113, 12643-12648, https://doi.org/10.1021/acscentsci.7b00452, 2016.

397 Liu, P., Li, Y. J., Wang, Y., Bateman, A. P., Zhang, Y., Gong, Z., Bertram, A. K. and
398 Martin, S. T.: Highly viscous states affect the browning of atmospheric
399 organic particulate matter, ACS Cent. Sci.,
400 https://doi.org/10.1021/acscentsci.7b00452, 2018.

401 Loza, C. L., Coggon, M. M., Nguyen, T. B., Zuend, A., Flagan, R. C. and Seinfeld, J.
402 H.: On the mixing and evaporation of secondary organic aerosol components,
403 Environ. Sci. Technol., 47, 6173-6180, https://doi.org/10.1021/es400979k,
404 2013.

405 Maclean, A. M., Butenhoff, C. L., Grayson, J. W., Barsanti, K., Jimenez, J. L. and
406 Bertram, A. K.: Mixing times of organic molecules within secondary organic
407 aerosol particles: a global planetary boundary layer perspective, Atmos. Chem.
408 Phys., 17, 13037-13048, https://doi.org/10.5194/acp-17-13037-2017, 2017.

409 Mai, H., Shiraiwa, M., Flagan, R. C. and Seinfeld, J. H.: Under what conditions can
410 equilibrium gas–particle partitioning be expected to hold in the atmosphere?,
411 Environ. Sci. Technol., 49, 11485-11491,
412 https://doi.org/10.1021/acs.est.5b02587, 2015.

413 Maria, S. F., Russell, L. M., Gilles, M. K. and Myneni, S. C. B.: Organic aerosol
414 growth mechanisms and their climate-forcing implications, Science, 306,
415 1921-1924, https://doi.org/10.1126/science.1103491, 2004.

416 Marshall, F. H., Miles, R. E., Song, Y.-C., Ohm, P. B., Power, R. M., Reid, J. P. and
417 Dutcher, C. S.: Diffusion and reactivity in ultraviscous aerosol and the
418 correlation with particle viscosity, Chem. Sci., 7, 1298-1308,
419 https://doi.org/10.1039/C5SC03223G, 2016.

420 Mu, Q., Shiraiwa, M., Octaviani, M., Ma, N., Ding, A., Su, H., Lammel, G., Pöschl,
421 U. and Cheng, Y.: Temperature effect on phase state and reactivity controls
422 atmospheric multiphase chemistry and transport of PAHs, Sci. Adv., 4,
423 https://doi.org/10.1126/sciadv.aap7314, 2018.

O'Meara, S., Topping, D. O. and McFiggans, G.: The rate of equilibration of viscous aerosol particles, Atmos. Chem. Phys., 16, 5299-5313, https://doi.org/10.5194/acp-16-5299-2016, 2016.

Pankow, J. F.: An absorption model of gas-particle partitioning of organic-compounds in the atmosphere, Atmos. Environ., 28, 185-188, https://doi.org/10.1016/1352-2310(94)90093-0, 1994.

Perraud, V., Bruns, E. A., Ezell, M. J., Johnson, S. N., Yu, Y., Alexander, M. L., Zelenyuk, A., Imre, D., Chang, W. L., Dabdub, D., Pankow, J. F. and Finlayson-Pitts, B. J.: Nonequilibrium atmospheric secondary organic aerosol formation and growth, Proc. Natl. Acad. Sci. U.S.A., 109, 2836-2841, https://doi.org/10.1073/pnas.1119909109, 2012.

Petters, M. D. and Kreidenweis, S. M.: A single parameter representation of hygroscopic growth and cloud condensation nucleus activity, Atmos. Chem. Phys., 7, 1961-1971, https://doi.org/10.5194/acp-7-1961-2007, 2007.

Petters, S. S., Kreidenweis, S. M., Grieshop, A. P., Ziemann, P. J. and Petters, M. D.: Temperature- and humidity-dependent phase states of secondary organic aerosols, Geophys. Res. Lett., 46, https://doi.org/10.1029/2018GL080563, 2019.

Pöhlker, C., Wiedemann, K. T., Sinha, B., Shiraiwa, M., Gunthe, S. S., Smith, M., Su, H., Artaxo, P., Chen, Q., Cheng, Y., Elbert, W., Gilles, M. K., Kilcoyne, A. L. D., Moffet, R. C., Weigand, M., Martin, S. T., Pöschl, U. and Andreae, M. O.: Biogenic potassium salt particles as seeds for secondary organic aerosol in the Amazon, Science, 337, 1075-1078, https://doi.org/10.1126/science.1223264, 2012.

Pye, H. O. T., Murphy, B. N., Xu, L., Ng, N. L., Carlton, A. G., Guo, H., Weber, R., Vasilakos, P., Appel, K. W., Budisulistiorini, S. H., Surratt, J. D., Nenes, A., Hu, W., Jimenez, J. L., Isaacman-VanWertz, G., Misztal, P. K. and Goldstein, A. H.: On the implications of aerosol liquid water and phase separation for organic aerosol mass, Atmos. Chem. Phys., 17, 343-369, https://doi.org/10.5194/acp-17-343-2017, 2017.

Reid, J. P., Bertram, A. K., Topping, D. O., Laskin, A., Martin, S. T., Petters, M. D., Pope, F. D. and Rovelli, G.: The viscosity of atmospherically relevant organic particles, Nat. Commun., 9, 956, https://doi.org/10.1038/s41467-018-03027-z, 2018.

Riedel, T. P., Lin, Y. H., Zhang, Z., Chu, K., Thornton, J. A., Vizuete, W., Gold, A. and Surratt, J. D.: Constraining condensed-phase formation kinetics of secondary organic aerosol components from isoprene epoxydiols, Atmos. Chem. Phys., 16, 1245-1254, https://doi.org/10.5194/acp-16-1245-2016, 2016.

Riipinen, I., Pierce, J. R., Yli-Juuti, T., Nieminen, T., Hakkinen, S., Ehn, M., Junninen, H., Lehtipalo, K., Petaja, T., Slowik, J., Chang, R., Shantz, N. C., Abbatt, J., Leaitch, W. R., Kerminen, V. M., Worsnop, D. R., Pandis, S. N.,

Donahue, N. M. and Kulmala, M.: Organic condensation: a vital link connecting aerosol formation to cloud condensation nuclei (CCN) concentrations, Atmos. Chem. Phys., 11, 3865-3878, https://doi.org/10.5194/acp-11-3865-2011, 2011.

Riipinen, I., Yli-Juuti, T., Pierce, J. R., Petaja, T., Worsnop, D. R., Kulmala, M. and Donahue, N. M.: The contribution of organics to atmospheric nanoparticle growth, Nat. Geosci., 5, 453-458, https://doi.org/10.1038/ngeo1499, 2012.

Roldin, P., Eriksson, A. C., Nordin, E. Z., Hermansson, E., Mogensen, D., Rusanen, A., Boy, M., Swietlicki, E., Svenningsson, B., Zelenyuk, A. and Pagels, J.: Modelling non-equilibrium secondary organic aerosol formation and evaporation with the aerosol dynamics, gas- and particle-phase chemistry kinetic multilayer model ADCHAM, Atmos. Chem. Phys., 14, 7953-7993, https://doi.org/10.5194/acp-14-7953-2014, 2014.

Rothfuss, N. E. and Petters, M. D.: Characterization of the temperature and humidity-dependent phase diagram of amorphous nanoscale organic aerosols, Phys. Chem. Chem. Phys., 19, 6532-6545, https://doi.org/10.1039/C6CP08593H, 2017.

Saha, P. K. and Grieshop, A. P.: Exploring divergent volatility properties from yield and thermodenuder measurements of secondary organic aerosol from α-pinene ozonolysis, Environ. Sci. Technol., 50, 5740-5749, https://doi.org/10.1021/acs.est.6b00303, 2016.

Saleh, R., Donahue, N. M. and Robinson, A. L.: Time scales for gas-particle partitioning equilibration of secondary organic aerosol formed from alpha-pinene ozonolysis, Environ. Sci. Technol., 47, 5588-5594, https://doi.org/10.1021/es400078d, 2013.

Seinfeld, J. H. and Pandis, S. N.: Atmospheric chemistry and physics - From air pollution to climate change, John Wiley & Sons, Inc., New York, 2006.

Shiraiwa, M., Ammann, M., Koop, T. and Poschl, U.: Gas uptake and chemical aging of semisolid organic aerosol particles, Proc. Natl. Acad. Sci. U.S.A., 108, 11003-11008, https://doi.org/10.1073/pnas.1103045108, 2011.

Shiraiwa, M., Pfrang, C., Koop, T. and Pöschl, U.: Kinetic multi-layer model of gas-particle interactions in aerosols and clouds (KM-GAP): linking condensation, evaporation and chemical reactions of organics, oxidants and water, Atmos. Chem. Phys., 12, 2777-2794, https://doi.org/10.5194/acp-12-2777-2012, 2012.

Shiraiwa, M. and Seinfeld, J. H.: Equilibration timescale of atmospheric secondary organic aerosol partitioning, Geophys. Res. Lett., 39, L24801, https://doi.org/10.1029/2012GL054008, 2012.

Shiraiwa, M., Yee, L. D., Schilling, K. A., Loza, C. L., Craven, J. S., Zuend, A., Ziemann, P. J. and Seinfeld, J. H.: Size distribution dynamics reveal

particle-phase chemistry in organic aerosol formation, Proc. Natl. Acad. Sci. U.S.A., 110, 11746-11750, https://doi.org/10.1073/pnas.1307501110, 2013a.

Shiraiwa, M., Zuend, A., Bertram, A. K. and Seinfeld, J. H.: Gas-particle partitioning of atmospheric aerosols: interplay of physical state, non-ideal mixing and morphology, Phys. Chem. Chem. Phys., 15, 11441-11453, https://doi.org/10.1039/C3CP51595H, 2013b.

Shiraiwa, M., Li, Y., Tsimpidi, A. P., Karydis, V. A., Berkemeier, T., Pandis, S. N., Lelieveld, J., Koop, T. and Pöschl, U.: Global distribution of particle phase state in atmospheric secondary organic aerosols, Nat. Commun., 8, 15002, https://doi.org/10.1038/ncomms15002, 2017.

Shrivastava, M., Cappa, C. D., Fan, J., Goldstein, A. H., Guenther, A. B., Jimenez, J. L., Kuang, C., Laskin, A., Martin, S. T., Ng, N. L., Petaja, T., Pierce, J. R., Rasch, P. J., Roldin, P., Seinfeld, J. H., Shilling, J., Smith, J. N., Thornton, J. A., Volkamer, R., Wang, J., Worsnop, D. R., Zaveri, R. A., Zelenyuk, A. and Zhang, Q.: Recent advances in understanding secondary organic aerosol: Implications for global climate forcing, Rev. Geophys., 55, 509-559, https://doi.org/10.1002/2016RG000540, 2017a.

Shrivastava, M., Lou, S., Zelenyuk, A., Easter, R. C., Corley, R. A., Thrall, B. D., Rasch, P. J., Fast, J. D., Simonich, S. L. M. and Shen, H.: Global long-range transport and lung cancer risk from polycyclic aromatic hydrocarbons shielded by coatings of organic aerosol, Proc. Natl. Acad. Sci. U.S.A., 114, 1246-1251, https://doi.org/10.1073/pnas.1618475114, 2017b.

Slade, J. H., Shiraiwa, M., Arangio, A., Su, H., Pöschl, U., Wang, J. and Knopf, D. A.: Cloud droplet activation through oxidation of organic aerosol influenced by temperature and particle phase state, Geophys. Res. Lett., 41, 5297-5306, https://doi.org/10.1002/2014GL060582, 2017.

Tröstl, J., Chuang, W. K., Gordon, H., Heinritzi, M., Yan, C., Molteni, U., Ahlm, L., Frege, C., Bianchi, F., Wagner, R., Simon, M., Lehtipalo, K., Williamson, C., Craven, J. S., Duplissy, J., Adamov, A., Almeida, J., Bernhammer, A.-K., Breitenlechner, M., Brilke, S., Dias, A., Ehrhart, S., Flagan, R. C., Franchin, A., Fuchs, C., Guida, R., Gysel, M., Hansel, A., Hoyle, C. R., Jokinen, T., Junninen, H., Kangasluoma, J., Keskinen, H., Kim, J., Krapf, M., Kürten, A., Laaksonen, A., Lawler, M., Leiminger, M., Mathot, S., Möhler, O., Nieminen, T., Onnela, A., Petäjä, T., Piel, F. M., Miettinen, P., Rissanen, M. P., Rondo, L., Sarnela, N., Schobesberger, S., Sengupta, K., Sipilä, M., Smith, J. N., Steiner, G., Tomè, A., Virtanen, A., Wagner, A. C., Weingartner, E., Wimmer, D., Winkler, P. M., Ye, P., Carslaw, K. S., Curtius, J., Dommen, J., Kirkby, J., Kulmala, M., Riipinen, I., Worsnop, D. R., Donahue, N. M. and Baltensperger, U.: The role of low-volatility organic compounds in initial particle growth in the atmosphere, Nature, 533, 527-531, https://doi.org/10.1038/nature18271, 2016.

546 Vaden, T. D., Imre, D., Beránek, J., Shrivastava, M. and Zelenyuk, A.: Evaporation
547 kinetics and phase of laboratory and ambient secondary organic aerosol, Proc.
548 Natl. Acad. Sci. U.S.A., 108, 2190-2195,
549 https://doi.org/10.1073/pnas.1013391108, 2011.

550 Virtanen, A., Joutsensaari, J., Koop, T., Kannosto, J., Yli-Pirilä, P., Leskinen, J.,
551 Mäkelä, J. M., Holopainen, J. K., Pöschl, U. and Kulmala, M.: An amorphous
552 solid state of biogenic secondary organic aerosol particles, Nature, 467,
553 824-827, https://doi.org/10.1038/nature09455, 2010.

554 Wang, J., Krejci, R., Giangrande, S., Kuang, C., Barbosa, H. M., Brito, J., Carbone,
555 S., Chi, X., Comstock, J. and Ditas, F.: Amazon boundary layer aerosol
556 concentration sustained by vertical transport during rainfall, Nature, 539,
557 416-419, https://doi.org/10.1038/nature19819, 2016.

558 Ye, Q., Robinson, E. S., Ding, X., Ye, P., Sullivan, R. C. and Donahue, N. M.:
559 Mixing of secondary organic aerosols versus relative humidity, Proc. Natl.
560 Acad. Sci. U.S.A., 113, 12649-12654,
561 https://doi.org/10.1073/pnas.1604536113, 2016.

562 Ye, Q., Upshur, M. A., Robinson, E. S., Geiger, F. M., Sullivan, R. C., Thomson, R.
563 J. and Donahue, N. M.: Following particle-particle mixing in atmospheric
564 secondary organic aerosols by using isotopically labeled terpenes, Chem, 4,
565 318-333, https://doi.org/10.1016/j.chempr.2017.12.008, 2018.

566 Yli-Juuti, T., Pajunoja, A., Tikkanen, O.-P., Buchholz, A., Faiola, C., Väisänen, O.,
567 Hao, L., Kari, E., Peräkylä, O., Garmash, O., Shiraiwa, M., Ehn, M., Lehtinen,
568 K. and Virtanen, A.: Factors controlling the evaporation of secondary organic
569 aerosol from α-pinene ozonolysis, Geophys. Res. Lett., 44, 2562-2570,
570 https://doi.org/10.1002/2016GL072364, 2017.

571 You, Y., Smith, M. L., Song, M., Martin, S. T. and Bertram, A. K.: Liquid–liquid
572 phase separation in atmospherically relevant particles consisting of organic
573 species and inorganic salts, Int. Rev. Phys. Chem., 33, 43-77,
574 https://doi.org/10.1080/0144235X.2014.890786, 2014.

575 Zaveri, R. A., Easter, R. C., Shilling, J. E. and Seinfeld, J. H.: Modeling kinetic
576 partitioning of secondary organic aerosol and size distribution dynamics:
577 representing effects of volatility, phase state, and particle-phase reaction,
578 Atmos. Chem. Phys., 14, 5153-5181,
579 https://doi.org/10.5194/acp-14-5153-2014, 2014.

580 Zaveri, R. A., Shilling, J. E., Zelenyuk, A., Liu, J., Bell, D. M., D'Ambro, E. L.,
581 Gaston, C. J., Thornton, J. A., Laskin, A., Lin, P., Wilson, J., Easter, R. C.,
582 Wang, J., Bertram, A. K., Martin, S. T., Seinfeld, J. H. and Worsnop, D. R.:
583 Growth kinetics and size distribution dynamics of viscous secondary organic
584 aerosol, Environ. Sci. Technol., 52, 1191-1199,
585 https://doi.org/10.1021/acs.est.7b04623, 2018.

586 Zhang, X., Pandis, S. N. and Seinfeld, J. H.: Diffusion-limited versus
587 quasi-equilibrium aerosol growth, Aerosol Sci. Technol., 46, 874-885,
588 https://doi.org/10.1080/02786826.2012.679344, 2012.

589 Zhang, Y., Chen, Y., Lambe, A. T., Olson, N. E., Lei, Z., Craig, R. L., Zhang, Z.,
590 Gold, A., Onasch, T. B., Jayne, J. T., Worsnop, D. R., Gaston, C. J., Thornton,
591 J. A., Vizuete, W., Ault, A. P. and Surratt, J. D.: Effect of the Aerosol-Phase
592 State on Secondary Organic Aerosol Formation from the Reactive Uptake of
593 Isoprene-Derived Epoxydiols (IEPOX), Environ. Sci. Technol. Lett.,
594 https://doi.org/10.1021/acs.estlett.8b00044, 2018.
595

Atmos. Chem. Phys. Discuss., https://doi.org/10.5194/acp-2019-76
Manuscript under review for journal Atmos. Chem. Phys.
Discussion started: 5 February 2019

Atmospheric Chemistry and Physics Discussions

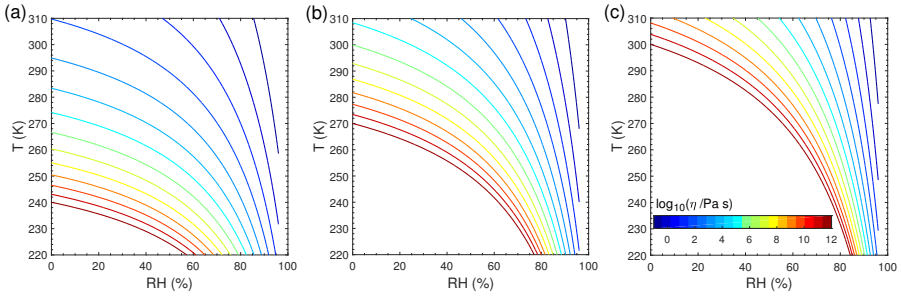

596

597 **Figure 1.** Viscosity of pre-existing particles as a function of temperature and relative
598 humidity. The glass transition temperatures under dry conditions ($T_{g,org}$) are (a) 240 K,
599 (b) 270 K, and (c) 300 K, respectively.

600

601

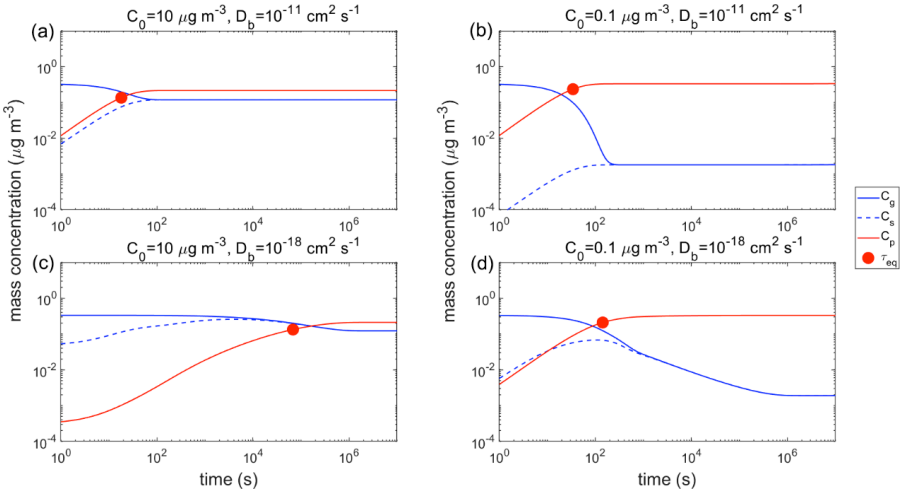

602

603 **Figure 2.** Temporal evolution of mass concentrations of the condensing compound Z
604 in the gas phase (C_g), just above the particle surface (C_s), and in the particle phase
605 (C_p). τ_{eq} is marked with the red circle. RH = 60% and T is (a–b) 298 K and (c–d) 250
606 K. The C_0 of Z is (a, c) 10 μg m^{-3} and (b, d) 0.1 μg m^{-3}. The glass transition
607 temperature of pre-existing particles under dry conditions ($T_{g,org}$) is set to be 270 K,
608 which leads to D_b of (a–b) 10^{-11} cm^2 s^{-1} and (c–d) 10^{-18} cm^2 s^{-1}. The initial mass
609 concentration of pre-existing particles is set to be 20 μg m^{-3} with the number
610 concentrations of 3×10^4 cm^{-3} and the initial particle diameter of 100 nm.

611

Atmos. Chem. Phys. Discuss., https://doi.org/10.5194/acp-2019-76
Manuscript under review for journal Atmos. Chem. Phys.
Discussion started: 5 February 2019

Atmospheric Chemistry and Physics Discussions

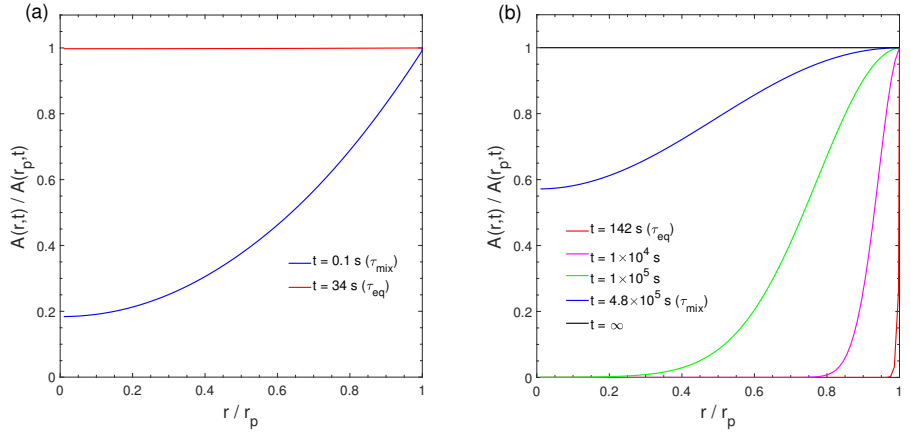

612

613 **Figure 3.** Dimensionless radial concentration profiles in the particle for the condensation of
614 the LVOC species (C_0 = 0.1 μg m^{-3}) at RH = 60% and (a) T = 298 K with D_b = 10^{-11} cm^2 s^{-1}
615 and (b) T = 250 K with D_b = 10^{-18} cm^2 s^{-1}. The x-axis indicates the radial distance from the
616 particle center (r) normalized by the particle radius (r_p), ranging from the particle core (r / r_p ≈
617 0) to the surface (r / r_p =1). The y-axis indicates the bulk concentration of the condensing
618 compound at a given position in the bulk (r) normalized by the bulk concentration at particle
619 surface (r_p).

620

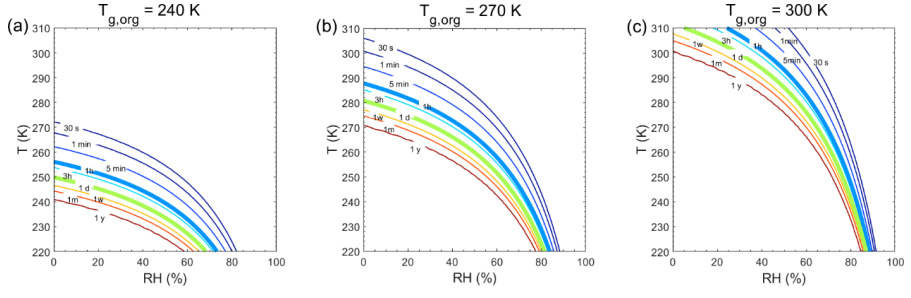

621

622 **Figure 4.** Equilibration timescale (τ_{eq}) as a function of temperature and relative
623 humidity. The glass transition temperatures of pre-existing particles at dry conditions
624 ($T_{g,org}$) are (a) 240 K, (b) 270 K, and (c) 300 K, respectively. The saturation mass
625 concentration (C_0) of the condensing compound is 10 μg m^{-3} (SVOC). The mass
626 concentration of pre-existing particles is set to be 20 μg m^{-3} with the number
627 concentrations of 3 × 10^4 cm^{-3} and the initial particle diameter of 100 nm.

628

Atmos. Chem. Phys. Discuss., https://doi.org/10.5194/acp-2019-76
Manuscript under review for journal Atmos. Chem. Phys.
Discussion started: 5 February 2019

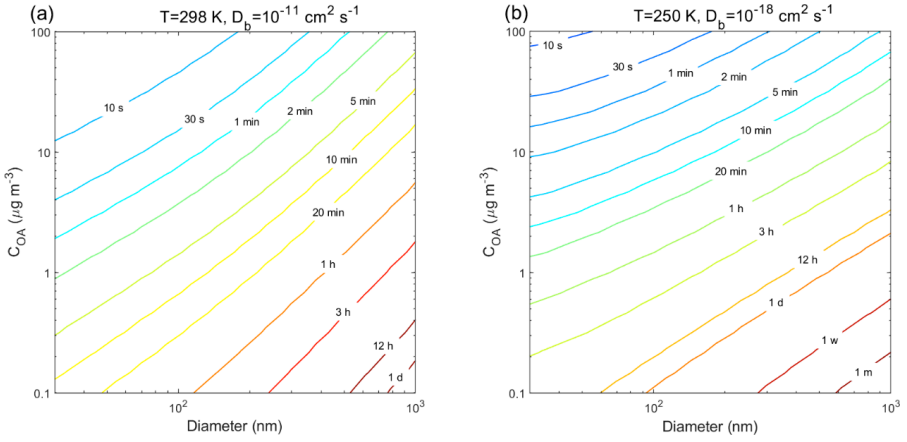

Figure 5. Equilibration timescale (τ_{eq}) for LVOC (C_0 = 0.1 μg m^{-3}) as a function of particle diameter (nm) and mass concentration (μg m^{-3}) of pre-existing particles at 60% RH and T of (a) 298 K and (b) 250 K. The glass transition temperature of pre-existing particles under dry conditions ($T_{g,org}$) is set to be 270 K, which leads to D_b of (a) 10^{-11} cm^2 s^{-1} and (b) 10^{-18} cm^2 s^{-1}.

Atmos. Chem. Phys. Discuss., https://doi.org/10.5194/acp-2019-76
Manuscript under review for journal Atmos. Chem. Phys.
Discussion started: 5 February 2019

Atmospheric Chemistry and Physics Discussions

636 **Appendix:**

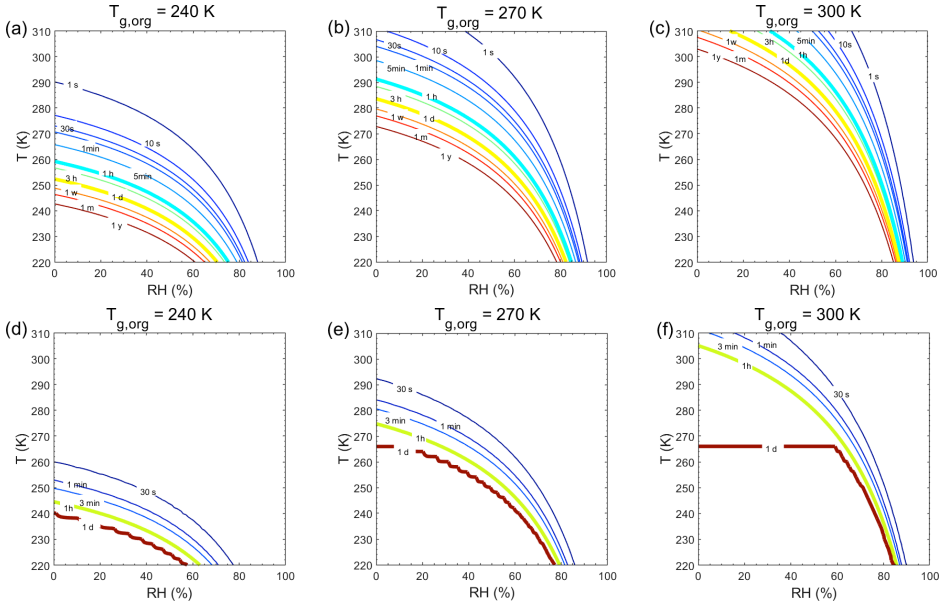

637

638

639 **Figure A1.** Equilibration timescale (τ_{eq}) as a function of temperature and relative
640 humidity. The glass transition temperatures of pre-existing particles at dry conditions
641 ($T_{g,org}$) are set to be (a, d) 240 K, (b, e) 270 K, and (c, f) 300 K. The mass
642 concentration of pre-existing particles is 20 μg m^{-3}. The saturation mass concentration
643 (C_0) of the condensing compound is (a, b, c) 10^3 μg m^{-3} and (d, e, f) 0.1 μg m^{-3}.

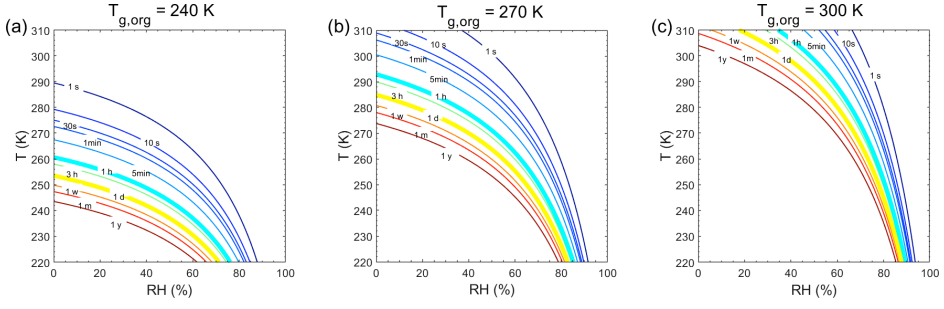

644

645 **Figure A2.** Mixing timescale (τ_{mix}) as a function of temperature and relative humidity.
646 The particle diameter is assumed to be 100 nm with the glass transition temperatures
647 of pre-existing particles at dry conditions ($T_{g,org}$) of (a) 240 K, (b), 270 K and (c) 300
648 K.

649